

An antioxidant system through conjugating superoxide dismutase onto metal-organic framework for cardiac repair

Jiacheng Guo^{a,b,1}, Zhenzhen Yang^{c,1}, Yongzheng Lu^{a,b,1}, Chunyan Du^d, Chang Cao^{a,b},
Bo Wang^{a,b}, Xiaoting Yue^{a,b}, Zenglei Zhang^{a,b}, Yanyan Xu^{a,b}, Zhen Qin^{a,b}, Tingting Huang^e,
Wei Wang^f, Wei Jiang^{g,***}, Jinying Zhang^{a,b,**}, Junnan Tang^{a,b,*}

^a Department of Cardiology, The First Affiliated Hospital of Zhengzhou University, Zhengzhou, Henan, 450052, China

^b Key Laboratory of Cardiac Injury and Repair of Henan Province, Zhengzhou, Henan, 450018, China

^c Department of Oncology, The First Affiliated Hospital of Zhengzhou University, Zhengzhou, Henan, 450052, China

^d Laboratory Animal Center, School of Medical Sciences, Zhengzhou University, Zhengzhou, Henan, 450052, China

^e Department of Polymer Science, College of Chemistry, Jilin University, Changchun, Jilin, 130012, China

^f Henan Medical Association, Zhengzhou, Henan, 450052, China

^g Academy of Medical Science, Zhengzhou University, Zhengzhou, Henan, 450052, China

ARTICLE INFO

Keywords:

Acute myocardial infarction
Immobilized enzyme
Reactive oxygen species
Nanomedicine

ABSTRACT

Acute myocardial infarction (AMI) remains a dominant origin of morbidity, mortality and disability worldwide. Increases in reactive oxygen species (ROS) are key contributor to excessive cardiac injury after AMI. Here we developed an immobilized enzyme with Superoxide Dismutase (SOD) activity cross-link with Zr-based metal-organic framework (ZrMOF) (SOD-ZrMOF) for mitigate ROS-caused injury. *In vitro* and *in vivo* evidence indicates that SOD-ZrMOF exhibits excellent biocompatibility. By efficiently scavenging ROS and suppressing oxidative stress, SOD-ZrMOF can protect the function of mitochondria, reduce cell death and alleviate inflammation. More excitingly, long-term study using an animal model of AMI demonstrated that SOD-ZrMOF can reduce the infarct area, protect cardiac function, promote angiogenesis and inhibit pathological myocardial remodeling. Therefore, SOD-ZrMOF holds great potential as an efficacious and safe nanomaterial treatment for AMI.

1. Introduction

Acute myocardial infarction (AMI), a dominant origin of death worldwide [1], involves myocardial injury and cardiomyocyte (CM) death caused by acute occlusion or severe stenosis of coronary arteries, resulting in local persistent ischemia and hypoxia. During the occurrence of AMI, lots of reactive oxygen species (ROS) are produced because of persistent hypoxia and lack of ATP in CMs [2,3]. This leads to activation of the apoptosis cascade reaction, CM death, and degradation and remodeling of cardiac extracellular matrix (ECM) [4]. Excessive ROS and necrotic CMs activate the immune system and produce a severe inflammatory response [5,6], which forms a vicious circle by promoting further elevation of ROS [6]. It is known that the inflammatory process

is the basis of the development and complications of myocardial infarction (MI). Appropriate inflammation is conducive to the repair of MI, while excessive inflammation leads to the secondary aggravation of myocardial injury [7]. This accelerates the occurrence of fibrotic microenvironment/left ventricular (LV) remodeling [8]. Then, over time, cardiac function deteriorates progressively, eventually leading to congestive heart failure [9].

ROS is an important part of the normal metabolic pathway and plays a certain role in cell signal transduction and homeostasis [10,11]. After MI, the blood supply of the heart is persistently blocked, resulting in irreversible injury to CMs, due to ischemia and hypoxia. Then, the production of ROS occurs. This is mainly attributed to the activation of xanthine oxidase in endothelial cells [12], the electron transport chain

Peer review under responsibility of KeAi Communications Co., Ltd.

* Corresponding author. No.1 Eastern Jianshe Road, Zhengzhou, Henan, 450052, China.

** Corresponding author. No.1 Eastern Jianshe Road, Zhengzhou, Henan, 450052, China.

*** Corresponding author. No.40 North Road, 27 District University, Zhengzhou, Henan, 450052, China.

E-mail addresses: weijiang@zzu.edu.cn (W. Jiang), jy Zhang@zzu.edu.cn (J. Zhang), fcctangjn@zzu.edu.cn (J. Tang).

¹ These authors contributed equally to this work.

<https://doi.org/10.1016/j.bioactmat.2021.08.019>

Received 18 March 2021; Received in revised form 5 August 2021; Accepted 16 August 2021

Available online 22 August 2021

2452-199X/© 2021 The Authors. Publishing services by Elsevier B.V. on behalf of KeAi Communications Co. Ltd. This is an open access article under the CC

BY-NC-ND license (<http://creativecommons.org/licenses/by-nc-nd/4.0/>).

reaction of mitochondria in CMs, and NADPH oxidation in inflammatory cells [13]. Among them, the mitochondrion appears to be the major source of ROS under physiological and pathophysiological conditions [14]. Continuous hypoxia will change the structure/dynamics of mitochondria and electron transfer complexes, and energy metabolism will be impaired. Cytochrome oxidase is unable to reduce oxygen to water, and an electron will be taken away by O_2 , resulting in harmful O_2^{\bullet} , which is the first ROS produced in organisms and the predecessor of all ROS. In addition, overproduced ROS would overwhelm the endogenous defense mechanisms (SOD, etc.), further leading to the accumulation of ROS [14,15]. ROS is considered to play a critical role in disease progression after MI [9]. It is known that ROS can directly damage cell and organelle membranes, leading to CM apoptosis and necrosis [4] as well as the increase of inflammatory cytokines [5], the degradation of ECM, and fibrotic microenvironment promotion. Elevated ROS can also promote inflammation and stabilize HIF-1 α by mediating the overexpression of NF- κ B during hypoxia. HIF-1 α has been shown to be a master transcription factor, regulating many hundreds of target genes in response to hypoxia [7,16,17]. Studies have shown that the death of CMs mainly occurs within 24 h of ischemia and hypoxia. Early ROS clearance can reduce CM death, lessen the generation of inflammatory factors and the degradation of ECM, and lower subsequent injury [18–20].

Although there are abundant circulating ROS-scavenging drugs, such as deferoxamine [21], *N*-acetylcysteine, and ascorbic acid [22], which are used intravenously, antioxidants may be cleared quickly, and generally, intravenous administration requires high concentrations to achieve local effective doses. These high doses can interfere with the normal physiological processes of other organs. Therefore, local application of efficient ROS scavengers and targeted delivery methods seem more attractive [18,19,23]. The main antioxidant defense system in the body includes superoxide dismutase (SOD), which can catalyze O_2^{\bullet} into H_2O_2 and oxygen [24]. However, many problems greatly restrict the application of natural SOD in therapy, such as high synthesis cost and non-specific targeting [25]. And the major obstruction to the widespread application is the easy inactivation of enzymes when exposed to high temperatures and/or nonaqueous media during machining, which can intermingle the special and intricate interactions of covalent and noncovalent that disrupt the stability of their tertiary structures under artificial conditions [26]. Several strategies have been used to overcome the vulnerability of enzymes, such as immobilization [27]. Immobilizing enzymes on the surface or inside of porous materials often permits easy separation of enzymes from their reaction products, which is a major advantage compared to dissolved enzymes reactions. Actually, biotechnology of immobilized enzymes has been applied *in vivo* and *in vitro* research [28]. The immobilization of enzymes by porous silicon has been a mature technology, while metal-organic framework (MOF) seems a better choice. Representing a recent species of support nanomaterial for enzymes, MOFs possess easy optimized chemical functionality and pore dimensions of a framework for the immobilization of specific enzymes under biocompatible synthesis conditions (H_2O , room temperature), which has a precision that can't be achieved by other porous materials and extensive scope for development [26]. However, to date, there is no application of immobilized enzyme in the cardiovascular field.

This study uses SOD as a raw material and reduces the size to produce a larger surface area to improve the efficiency of the catalytic reaction. By using a well-organized crystalline Zr-based MOF (ZrMOF) as a precursor, we found that the immobilized enzyme becomes uniformly dispersed and more stable. Through intramyocardial injection, these stabilized immobilized enzymes were for the first time applied to study the repair of myocardial injury after MI.

2. Methods

2.1. Materials

SOD, $ZrCl_4$, acetic acid, terephthalic acid, *N,N*-Dimethylformamide (DMF), 3,3',5,5'-tetramethylbenzidine (TMB), fluorescein isothiocyanate (FITC), 2,2'-Azinobis-(3-ethylbenzthiazoline-6-sulphonate) (ABTS), and H_2O_2 were purchased from Sigma-Aldrich.

2.2. Construction of SOD-ZrMOF

ZrMOF was synthesized as in previous reports [29]. With the assistance of ultrasound for about 1 min, $ZrCl_4$ (0.0668 g, 0.3 mmol) and 1.38 mL of the modulator (acetic acid) were dissolved in DMF (10 mL). The linker was put into the clear solution in equimolar ratio relative to $ZrCl_4$ (0.0543 g, 0.3 mmol) and dissolved. The reaction sample was put in an oven and kept to react for 24 h at 120 °C, then regressed to room temperature. The precipitation was acquired through 5 min centrifugation under 8000 rpm and suspended again in 10 mL DMF. The suspension was continuously agitated at room temperature for around 12 h and centrifuged at 8000 rpm for 5 min. The precipitate was washed with ethanol (50 mL), water (50 mL), and dichloromethane (50 mL) to acquire the white solid UiO-66-NH $_2$ (ZrMOF), which was lyophilized and then dried under decompression. The as-prepared ZrMOF (25 mg) was ultrasonically mixed with SOD (6 mg) in 2 mL phosphate buffered saline (PBS) for 10 min at a power density of 80 W, next added 8 mL of 100% saturated ammonium sulfate solution to precipitate the SOD under magnetic stirring for 20 min at 4 °C. Then an appropriate amount of 25% glutaraldehyde (GA, as the cross-linker) was adding into the above mixture drop by drop. After cross-linking for 90 min, the SOD-ZrMOF was washed three times with 10 mL PBS containing 10% glucose (m/V) and stored at 4 °C for subsequent use.

2.3. Enzyme activity detection

The enzyme activity of SOD-ZrMOF and free SOD were measured using a SOD assay kit (Solarbio, China). The absorbance at 560 nm was measured using a quartz colorimetric dish reader after incubating at 37 °C for 30 min.

2.4. Synthesis steps of FITC-SOD and FITC-SOD-ZrMOF

The labeling of SOD using FITC was conducted according to the previous report [30]. Briefly, SOD (100 mg) and FITC (50 mg) were dissolved in 30 mL of phosphate buffer (50 mM, pH 8.0), and the sample was stirred with a speed of 180 rpm at ambient temperature for 24 h. Then the sample was dialyzed against distilled water for 3 days (molecular weight cut-off: 1000 Da) and lyophilized to obtain FITC-SOD. The composite FITC-SOD-ZrMOF was synthesized as described above, using FITC-SOD to replace SOD.

2.5. Characterization

Scanning electron microscopy (SEM) pictures were taken with an acceleration voltage of 3 kV (Hitachi S-4800 FE-SEM). And transmission electron microscopy (TEM) pictures were taken with JEM-2100F filed emission electron microscope. After dispersed in deionized water, the Zeta diameter and potential of ZrMOF and SOD-ZrMOF were detected via dynamic light scattering (DLS) (Malvern Zetasizer Nano ZS90). Confocal fluorescence images of SOD-ZrMOF labeled by FITC were detected by confocal laser scanning microscopy (CLSM) (Zeiss LSM 710).

2.6. Cell lines and cell culture

H9c2 rat CMs were achieved from the Cell Bank at the China

Academy of Sciences and cultured in high-glucose Dulbecco's Modified Eagle Medium (DMEM; Biological Industries, Israel) supplemented with 10% fetal bovine serum (FBS) (Biological Industries, Israel) and 1% penicillin/streptomycin (Solarbio, Beijing, China) at 37 °C, 5% CO₂ partial pressure and 95% relative humidity.

2.7. Cytotoxicity evaluation by CCK-8 assay

After seeded in a 96-well culture plate at the density of 4×10^3 cells per well, H9c2 cells were put in an incubator at 37 °C, 5% CO₂ partial pressure and 95% relative humidity for 24 h. For cytotoxicity assessment, culture media solutions of SOD-ZrMOF with different concentrations (0, 1, 5, 10, 15, 20, 30, 50, 70, and 90 µg/mL) were then added to all wells (n = 5). Cells treated with no SOD-ZrMOF were selected as control group. After co-incubation for 24 h or 48 h, 10% (v/v) cell counting kit reagent (CCK-8, Dojindo, Kumamoto, Japan) was added into all the wells followed by reaction in the dark for 2 h at 37 °C. Then the solution was detected at 450 nm via spectrophotometer.

2.8. Cell viability under a hypoxic environment in vitro

To analyze the effect of ZrMOF or SOD-ZrMOF on CMs under a hypoxic environment, the H9c2 cells (8×10^3 /well) were sowed in 96-well plates followed by culture for 24 h. When cells reached about 80% confluence in culture, culture media solutions of SOD-ZrMOF with different concentrations (0, 1, 5, 10, 15, 20, 30, 50, 70, and 90 µg/mL) were added to all wells. H9c2 cells were cultured in a hypoxia chamber (37 °C, 94% N₂, 5% CO₂, 1% O₂) for 12 h. Then the cell viability was measured by CCK-8 assay.

2.9. ROS detection by DCFH-DA probe

The ROS levels of H9c2 cells were detected through Reactive Oxygen Species Assay Kit (Beyotime Biotechnology, Nanjing, China). Briefly, the H9c2 cells (1×10^4 /well) were seeded in a 1µ-Slide 8 well ibiTreat (ibidi GmbH, Klopferspitz, Martinsried, Germany) followed by normal culture for 24 h and then exposed to culture media solutions with or without 20 µg/mL of ZrMOF or SOD-ZrMOF in a hypoxic environment for 12 h. Following the treatment, the supernatants were discarded, and cells were incubated with 2',7'-dichlorofluorescein-diacetate (DCFH-DA) for 40 min at 37 °C and then Hoechst (Beyotime Biotechnology, Nanjing, China) for 20 min. Cells were inspected using confocal laser scanning microscopy (Nikon, A1+R, Tokyo, Japan) and detected at 460 nm emission for Hoechst and 525 nm for DCFH-DA.

2.10. Depolarization ratio of mitochondrial membrane potential detection via JC-1 probe

The depolarization ratio of mitochondrial membrane potential (MMP) was measured via JC-1 probe (Beyotime Biotechnology, Nanjing, China). Cells (3×10^5 /well) were sowed into 6-well plates followed by normal culture for 24 h and then co-incubated with or without SOD-ZrMOF in a hypoxia chamber (37 °C, 94% N₂, 5% CO₂, 1% O₂) for 12 h. After cultivation, the cells were harvested and loaded with JC-1 (5 µg/mL) and placed at 37 °C for 25 min. The emissions of JC-1 monomer (green fluorescence) and aggregate (orange fluorescence) were at 529 nm and 590 nm, and the excitations were separately at 514 nm and 585 nm. Analyze the samples by flow cytometry (Becton Dickinson, Franklin Lakes, NJ, USA) with measuring green fluorescence emission in FITC channel and orange fluorescence emission in PE channel.

2.11. Western blot

H9c2 cells (3×10^5 /well) were sowed into 6-well plates, cultured for 24 h and then co-incubated with or without SOD-ZrMOF in a hypoxic environment for 12 h. After cultivation, cells were lysed using RIPA

lysing buffer (Beyotime Biotechnology, Nanjing, China) supplemented with phosphatase inhibitor and protease inhibitor, and the concentration of protein samples were detected via BCA protein assay kit (Solarbio, Beijing, China). Myocardial tissue samples were prepared in the same way as cell samples. Then, protein samples were separated via SDS-PAGE and blotted onto PVDF membranes, which were incubated with primary antibodies against HIF-1α (Abcam, USA, ab179483), phospho-NF-κB (Cell Signaling Technology, USA, #3033), NF-κB (Cell Signaling Technology, USA, #8242) and GAPDH (Abcam, USA, ab9485) for 2 h at room temperature and followed by secondary antibodies for 1 h.

2.12. Live/dead cell staining

Dead and live cells were separately observed via ethidium homodimer-1 (EthD-1) and calcein acetoxyethyl ester (calcein AM) (Invitrogen, Eugene, OR, USA). In short, H9c2 cells were sowed into 6-well plates and cultured for 24 h. After the same steps, the culture medium was abandoned, and the cells were washed gently with PBS. EthD-1 (3 µM) and Calcein AM (1.5 µM) were added into each well to stain H9c2 cells for 30 min at 37 °C in the darkness. Then the cells were washed again and observed using fluorescence microscopy (IX71, Olympus, Japan). EthD-1 fluoresced red and Calcein AM fluoresced green.

2.13. Apoptosis detection

Annexin V-FITC/PI double staining was chose to determine the inhibitory effect of SOD-ZrMOF on cell apoptosis under hypoxia. After the same steps, the cells were acquired and washed with cold PBS, resuspended with $1 \times$ binding buffer, and stained with 5 µL PI and 5 µL Annexin V-FITC (BD Biosciences, Piscataway, NJ, USA) following the instructions of the manufacturer. Then the cells were detected by flow cytometry (Becton Dickinson) via FlowJo software.

2.14. Animal studies

All animal experiments were carried out according to the guidelines established by the Welfare and Ethics Review Committee of Zhengzhou University Laboratory Animal Center (Approval number: ZZU-LAC20200925[02]). Male C57/BL6 mice (8–12 weeks old, 17–22 g) were used for the MI model and acquired from the Laboratory Animal Center of Zhengzhou University (Zhengzhou, China). Mice were housed at 25 °C under a 12-h light/dark cycle. Purified water and normal diet were available ad libitum before and after surgery preparation. Mice were adapted to the laboratory environment for 1 week before the experiments.

2.15. In vivo imaging

To identify the action time of SOD and SOD-ZrMOF *in vivo*, mice were intramyocardially injected with free FITC-SOD (5.5 µg/ml, 50 µl) or FITC-SOD-ZrMOF (20 µg/ml, 50 µl). We sacrificed the mice at three time points: 0, 1 and 4 h (n = 3 per time point). Immediately, the hearts were harvested and imaged using IVIS Spectrum(PerkinElmer).

2.16. Myocardial infarction model

After intraperitoneal injection of pentobarbital for general anesthesia, mice received endotracheal intubation and were artificially ventilated with room air. The hearts were exposed through a left fourth intercostal space thoracotomy, followed by ligation of the left anterior descending artery (LAD) at 1–2 mm below the inferior margin of the left atrial appendage with a 6-0 silk suture, and a rapid color change (becoming pale) of the left ventricular anterior wall confirmed the occlusion of the LAD. Then the heart obtained one of the below treatments:

1) intramyocardial injection of 50 μL PBS; 2) intramyocardial injection of 50 μL solution (20 $\mu\text{g}/\text{mL}$) of SOD-ZrMOF immediately after MI. Besides, we performed sham operations on mice without LAD occlusion. Then, the chest cavity, muscles and skin were stitched layer by layer with 4-0 silk sutures, and the mice were placed on the insulation blanket. After the mice resumed normal breathing, the endotracheal tube was removed. Finally, the mice were moved back to their cages after they were completely awake.

2.17. Serum biochemical test

To investigate the acute toxicity of SOD-ZrMOF *in vivo*, SOD-ZrMOF (1 μg in 50 μL) or PBS (50 μL) was intramyocardially injected into mice, followed by normal housing and feeding for 72 h ($n = 5$). Then, the blood samples were collected and the serum samples were gathered after centrifugation. Indexes of liver function (Alanine aminotransferase, ALT; Aspartate aminotransferase, AST), kidney function (Blood urea nitrogen, BUN; Creatinine, CREA), and myocardial enzymes (Creatine kinase, CK; Creatine Kinase, MB Form, CK-MB) were detected by an automatic biochemical analyzer (Chemray 240 or 840, Rayto, China). To determine the influence of SOD-ZrMOF on inflammatory response after MI, SOD-ZrMOF (1 μg in 50 μL) or PBS (50 μL) was intramyocardially injected into MI model mice. After the same operation process, serum samples were gathered one day later ($n = 5$). The levels of inflammatory factors (IL-6 and TNF- α) were detected using a Mouse TNF alpha ELISA Kit (Elabscience, E-EL-M0049c, China) and IL-6 Mouse Uncoated ELISA Kit (Invitrogen, #88-7064-22, USA), according to the manufacturers' instructions.

2.18. Echocardiography

After anesthetized using an isoflurane and oxygen mixture, mice underwent transthoracic echocardiography at 1 d before MI (baseline), 1 week, 2 weeks and 4 weeks after MI ($n = 6$). Cardiac functional parameters were measured by a mouse cardiologist blinded with respect to the experimental design via a Vevo 2100 Imaging System (VisualSonics, Toronto, Canada) and captured with an MS-550D probe. And the hearts were imaged in two dimensions along the long axis, at the section of the longest left ventricle diameter. The under formula was chose to calculate the ejection fraction (EF): $(\text{LVEDV} - \text{LVESV}/\text{LVEDV}) \times 100\%$.

2.19. Immunohistochemistry

Heart cryosections were fixed with 4% paraformaldehyde, permeabilized with 0.1% Triton X-100 in PBS, and blocked with 3% BSA solution. They were then incubated with the following antibodies: rabbit anti-HIF-1 α monoclonal antibody (1:500, Abcam, ab179483), mouse anti-CD31 monoclonal antibody (1:500, Abcam, ab24590), and rabbit anti-alpha smooth muscle actin (α -SMA) antibody (1:300, Abcam, ab5694). Then, fluorescent dye-conjugated secondary antibodies (Beyotime Biotechnology; Alexa Fluor 488 or Alexa Fluor 647) were used for the detection of above-mentioned primary antibodies. For cell apoptosis assays, TUNEL solution (Roche Diagnostics GmbH, REF 11684817910, Mannheim, Germany) were used to incubate with heart cryosections. Then, nuclei were stained with DAPI, and images were taken via a fluorescent microscope (Olympus BX53, Tokyo, Japan).

2.20. Histology analysis

After fixation with 4% paraformaldehyde for 24 h, sections of different organs were stained with hematoxylin and eosin (HE) to observe the damage to different organs and measure the percentage of MI area and the thickness of the left ventricle (LV) ($n = 6$). Using a HT15 trichrome staining (Masson) kit, Masson's trichrome staining was carried out to detect the percentage of viable myocardium. The degree of cardiac fibrosis was analyzed by sirius red staining ($n = 6$). Images of HE

and Masson were taken by Olympus BX53 microscope, and images of sirius red staining were taken with a polarization microscope (NIKON Eclipse Ci, Tokyo, Japan).

2.21. Statistical analysis

All data are expressed as mean \pm standard deviation (SD). Statistical analyses were performed with GraphPad Prism 5 software. Statistical significance was assessed at $P < 0.05$.

3. Results and discussion

3.1. Characterization of SOD-ZrMOF

Through the crosslinking approach shown in Fig. 1A, SOD was conjugated onto a porous nanomaterial, ZrMOF, which was synthesized by the solvothermal method. The morphology of composite SOD-ZrMOF was characterized via SEM and TEM (Fig. 1B–E). The images of SEM obviously demonstrated that, similar to blank ZrMOF, SOD-ZrMOF owned uniform and regular octahedron morphology. The average non-encapsulated SOD particle size was approximately 96 nm, while the value for SOD-ZrMOF was measured to be 154 nm and slightly bigger than ZrMOF (133 nm) as shown through the DLS method (Figure S1). These results were probably caused by the conjugation of SOD in the interface. The TEM images of SOD-ZrMOF also represented the identical morphology, demonstrating that the SOD loading did not influence the morphology of ZrMOF.

Then, the composite FITC-SOD-ZrMOF was investigated via CLSM scanning manner in layers to track the particle status at different depths along the position of z-axis (Fig. 2). Obviously, the fluorescence intensity of FITC showed a gradually increasing trend from the peak to the middle and then reduced to the bottom, which supplied a direct testimony for the SOD loading on ZrMOF. In addition, as shown in Figure S2, the enzyme activity of SOD-ZrMOF still kept a high level compared with free SOD (remain 83.16%).

3.2. Cytotoxic effect *in vitro*

After culturing for 24 and 48 h, the cytotoxicity in H9c2 cells incubated with ZrMOF (1, 5, 10, 15, 20, 30, 50, 70, or 90 $\mu\text{g}/\text{mL}$) or PBS was evaluated by CCK-8 assay, which proved the good biocompatibility of ZrMOF (Figure S3). Subsequently, under the same conditions, the cytotoxicity of SOD-ZrMOF was evaluated. As shown in Fig. 3A, although there was a statistical difference in the decrease of cell viability between the groups with SOD-ZrMOF concentration ≥ 70 $\mu\text{g}/\text{mL}$ on the first day and the groups ≥ 50 $\mu\text{g}/\text{mL}$ on the second day, the cell viability remained above 70% even at high drug concentrations up to 90 $\mu\text{g}/\text{mL}$. According to the ISO 10993-5 (Biological evaluation of medical devices, part 5: Test for *in vitro* cytotoxicity), in comparison with the control group, a decrease in cell viability of more than 30% is identified as a cytotoxic effect. Interestingly, SOD-ZrMOF showed a tendency to promote proliferation at low concentrations (1–10 $\mu\text{g}/\text{mL}$). All these data indicate that SOD-ZrMOF has low toxicity to normal CMs.

3.3. Effect on cell viability *in vitro*

After hypoxia for 12 h with different concentrations of SOD-ZrMOF, the cell viability was measured via CCK-8 assay. In the 0 $\mu\text{g}/\text{mL}$ group, cell viability was distinctly lower than in the non-hypoxia group, and nearly 50% of cells were killed, which means that 12 h of hypoxia was suitable in this test (Fig. 3B). In addition, under hypoxic conditions, cell viability was enhanced in a concentration-dependent style (in the 1–50 $\mu\text{g}/\text{mL}$ concentration groups) compared with the 0 $\mu\text{g}/\text{mL}$ group, indicating a highly effective anti-injury effect. However, in the 70 and 90 $\mu\text{g}/\text{mL}$ groups, we observed that the cell viability began to decrease, and there was no longer any obvious difference in the 90 $\mu\text{g}/\text{mL}$ group.

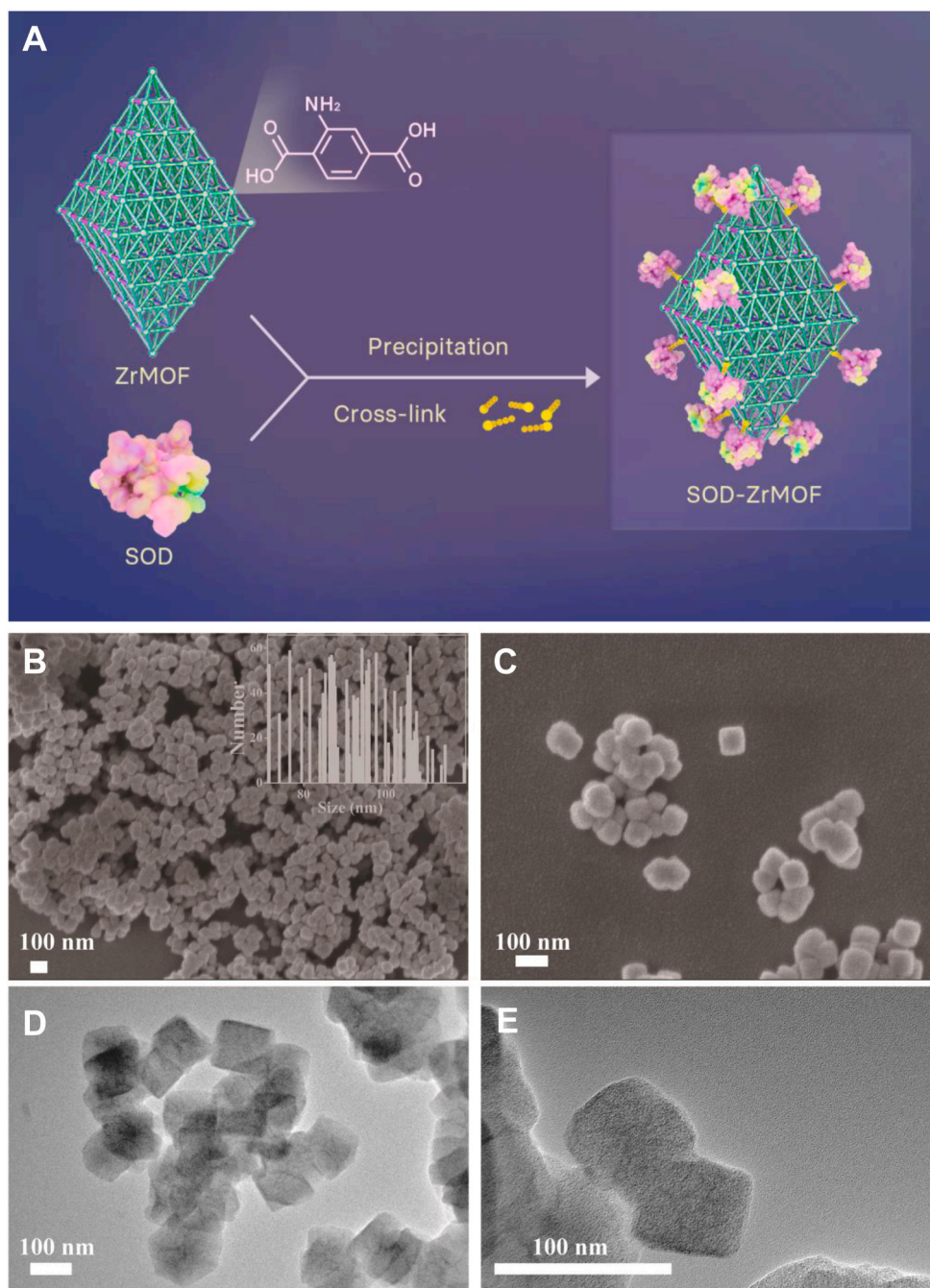


Fig. 1. Schematic of the construction of SOD-ZrMOF via physical absorption approach (A), SEM (B and C) and TEM (D and E) of ZrMOF and SOD-ZrMOF. Scale bar: 100 nm.

Since the 20 $\mu\text{g}/\text{mL}$ group performed outstandingly in both trials, this concentration was selected for further study.

3.4. Efficacy of ROS scavenging under hypoxia

As the foremost intermediates for oxidative stress, bursts of ROS occur in the microenvironment of the myocardium under hypoxic conditions [4]. These bursts directly destroy cell membranes and organelle membranes, proteins and DNA resulting in an imbalance of MMP, CM apoptosis and necrosis, and even the degradation of extracellular matrix to promote myocardial fibrosis. Therefore, the potency of nanoparticles to prevent hypoxic injury in H9c2 cells was evaluated. The ROS generation of H9c2 cells was revealed by the DCFH-DA ROS probe. As shown in Fig. 3C, after 12 h of hypoxia culture, the ROS level of H9c2 cells was

significantly enhanced. However, the cells treated with SOD-ZrMOF displayed a significant drop in ROS level (Figure S4). And it's worth mentioning that ZrMOF does not contribute to the antioxidant activation (Figure S5).

3.5. Protection against ROS-Induced oxidative stress

The regulation of mitochondrial metabolism is crucial for cellular functions, and in the case of the heart, mitochondria supply 90% of their energy through oxidative phosphorylation [31]. During ischemia, intracellular changes, including the disruption of MMP [32], lead to the generation of ROS, which then conversely aggravates mitochondrial damage. MMP is regarded as an important indicator of oxidative stress damage. Therefore, represented by the ratio of orange fluorescence to

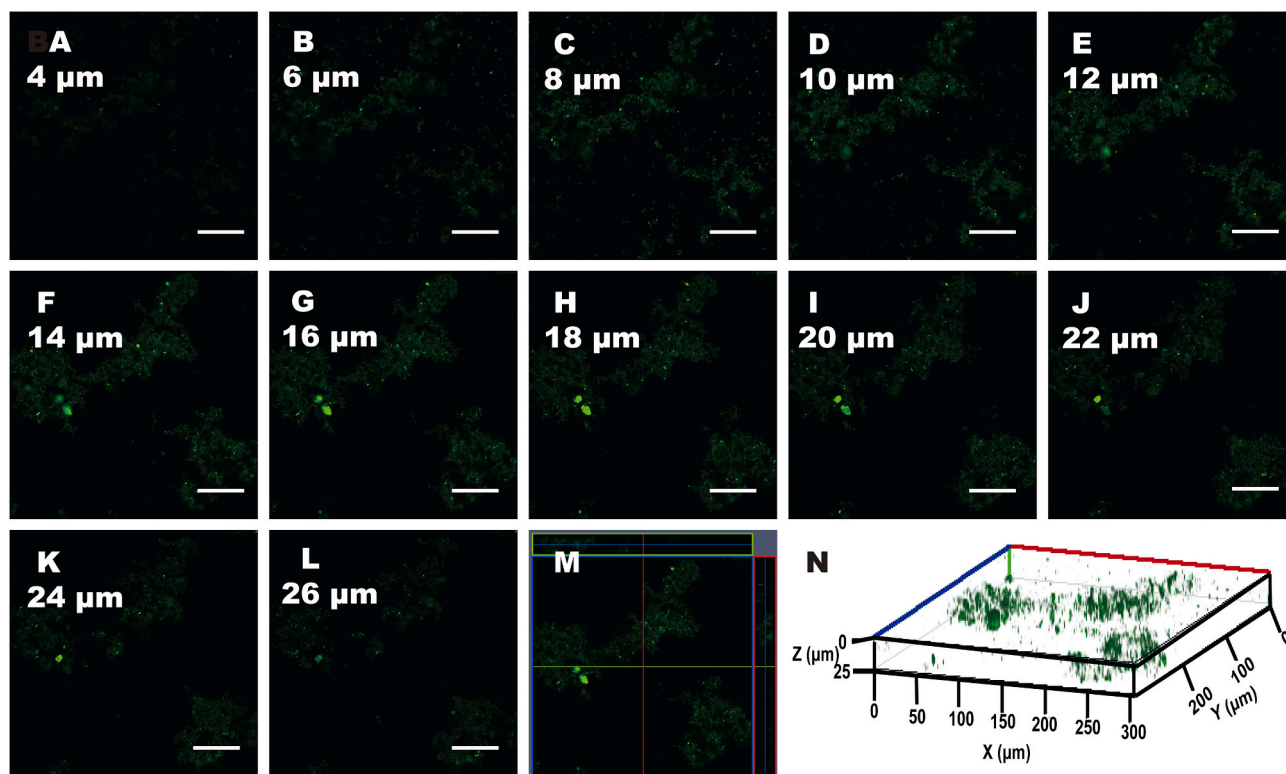


Fig. 2. FITC-SOD-ZrMOF images scanning in layers along the z-axis position via CLSM (A–L). The photograph M and N separately represent the 3D picture and homologous 3D reconstructed picture for above images. Scale bar: 200 μm .

green, the MMP depolarization ratio was detected by flow cytometry using a JC-1 probe. As shown in Fig. 4A and Figure S6, orange fluorescence-positive (PE+) cells reduced, while cells with green fluorescence (FITC+) markedly increased, in the hypoxia group compared with the control group, showing that hypoxic stimulation significantly led to an imbalance of MMP. In the therapy group treated with SOD-ZrMOF, the hypoxic damage to mitochondria was significantly reversed.

Apoptosis and necrosis, closely related to ROS overexpression and MMP disruption [33], are the main forms of myocardial cell death caused by MI. It is precisely because the regenerative capacity of CMs is not sufficient to compensate for the cell loss caused by MI that this disease is so deadly. Therefore, in the treatment of MI, it is extremely important to ensure that more cells survive. So as to further illustrate the protective effect of SOD-ZrMOF in this process, the death of H9c2 cells was determined by live/dead cell staining. As shown in Figure S7, the number of EthD-1-positive cells (red fluorescence, marking dead cells) increased after exposure to hypoxia compared with the control group, while in the SOD-ZrMOF group, this change was obviously suppressed.

In addition, to check the results of live/dead cell assay, apoptotic and necrotic H9c2 cells were analyzed by Annexin V-FITC/PI double staining. As shown in Fig. 4B and Figure S8, both apoptotic (Annexin V+/PI-) and necrotic (Annexin V+/PI+) cells were soared under hypoxia. Encouragingly, compared with the hypoxic group, there was a significant decrease in both apoptotic and necrotic cells with SOD-ZrMOF treatment.

NF- κB is a crucial molecular switch for oxidative stress response of cells. Prolonged activation of NF- κB may trigger inflammation by enhancing the roles of interleukin-1, interleukin-6 (IL-6) and tumor necrosis factor α (TNF- α), leading to endoplasmic reticulum stress responses and cell death [34]. Similarly, the hypoxia factor HIF-1 α could be also excessively activated with a prolonged duration under hypoxia. These HIF-1 α elevations can result in contractile impairment and cardiomyopathy [35]. Previous studies have shown that hypoxic stress

stimulates ROS accumulation [36], which is essential for HIF-1 α gene induction mediated by NF- κB [17,37,38]. ROS have been demonstrated to inhibit the proteolytic degradation of HIF-1 α [39]. In this situation, high levels of HIF-1 α can further stimulate ROS formation [38], leading to more extensive oxidative stress. However, inhibition of ROS formation can decrease HIF-1 α protein expression [40]. Consistently, we found that hypoxia enhanced the expression of NF- κB as well as HIF-1 α (Fig. 4C–E). Meanwhile, the cells treated with SOD-ZrMOF displayed a significant drop in the expression of NF- κB and HIF-1 α , signifying that SOD-ZrMOF successfully inhibited the expansion of the NF- κB /HIF-1 α pathway in oxidative stress during hypoxia.

These multiple lines of evidence indicate that incubating CMs with SOD-ZrMOF can reduce oxidative stress to protect mitochondrial function and decrease both apoptosis and necrosis by inhibiting the NF- κB /HIF-1 α pathway under hypoxia (Fig. 4F).

3.6. Acute toxicity evaluation of SOD-ZrMOF *in vivo*

Any latent toxicity from SOD-ZrMOF was evaluated by detecting relevant hematological parameters and HE staining of the major organs. Specifically, SOD-ZrMOF (1 μg in 50 μL) or PBS (50 μL) was intramyocardially injected into mice, followed by normal housing and feeding for 72 h. Then, the organs and blood samples were collected. Major organs images of HE staining (lung, heart, liver, kidney and spleen) are shown in Figure S9. In comparison with the PBS group, no clear histological changes were detected in any organs after SOD-ZrMOF administration. Correspondingly, no cardiac toxicity, renal toxicity, or hepatotoxicity from SOD-ZrMOF was found in the blood samples (Figure S10a–f). As both the results of HE staining and blood parameters indicated extremely low toxicity *in vivo*, we planned to continue follow-up experiments to verify the protective effect of SOD-ZrMOF on infarcted myocardium in mice.

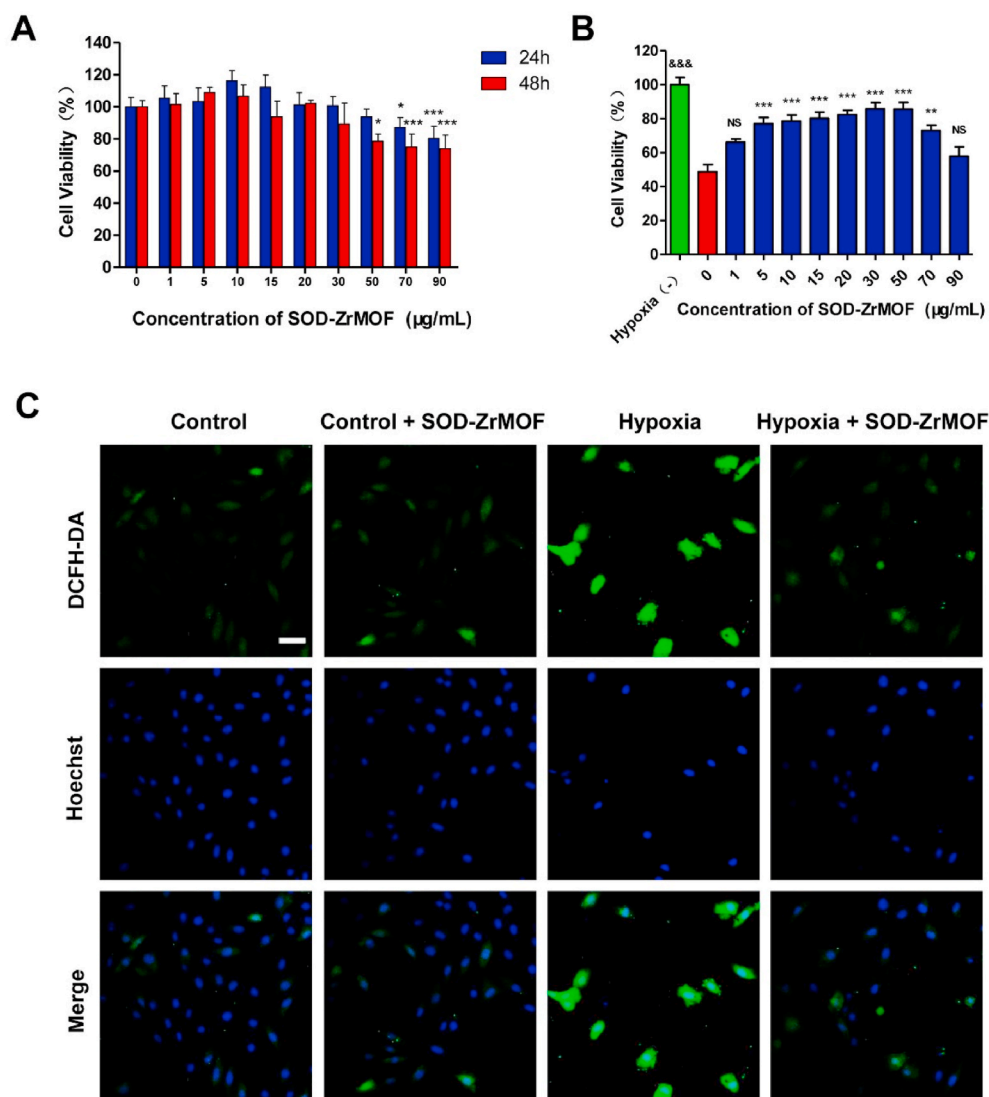


Fig. 3. Cytotoxicity, cell viability and ROS scavenging of SOD-ZrMOF *in vitro*. (A) The cytotoxicity of H9c2 cells with different concentrations of SOD-ZrMOF was assessed by CCK-8 after 24 h and 48 h of culture. Mean \pm SD, $n = 5$. * $P < 0.05$ and *** $P < 0.001$ in comparison with the 0 $\mu\text{g/mL}$ group. (B) The protective effect of H9c2 cells with different concentrations of SOD-ZrMOF was assessed by CCK-8 after 12 h of hypoxia. Mean \pm SD, $n = 5$. NS means no significance, ** $P < 0.01$ and *** $P < 0.001$ in comparison with the hypoxic group. (C) The level of ROS was measured by DCFH-DA probe (scale bar: 50 μm , $n = 3$).

3.7. Efficacy of SOD-ZrMOF in short-term cardiovascular disease model mice

Previous studies have shown that the half-life of SOD is very short, only a few minutes in mice, so it requires repeated local injections with a high-dose to make it possible of a therapeutic effect in animals or humans [41–43]. However, repeated intramyocardial injections in MI model mice are not feasible. Encouragingly, the *in vivo* imaging experiment in this study proved that SOD-ZrMOF could prolong the action time of SOD in heart (Figure S11).

We next used MI model mice to test the *in vivo* efficacy of SOD-ZrMOF. The entire design of animal study is shown in Fig. 5A. To detect the biological function in short-term MI mice, SOD-ZrMOF (1 μg in 50 μL) or PBS (50 μL) was intramyocardially injected into mice immediately after permanent coronary artery occlusion, followed by normal housing and feeding for 24 h. Then, the hearts and blood samples were collected to complete Western blot, immunohistochemistry staining, TdT-mediated dUTP nick-end labeling (TUNEL) and ELISA.

As illustrated in Fig. 5B and C, the HIF-1 α expression in the infarct area was analyzed by Western blot and immunohistochemistry staining 24 h after MI. In comparison with the sham group, the HIF-1 α expression was significantly increased in all experimental groups 24 h after infarction. Similar to the results of *in vitro* experiments, the addition of HIF-1 α expression was significantly suppressed with SOD-ZrMOF

treatment, meaning that intramyocardial injection of SOD-ZrMOF relieved the oxidative stress in the infarct area by eliminating ROS (Figure S12–13).

To further investigate the anti-inflammatory effect of SOD-ZrMOF through suppressing oxidative stress, the inflammatory cytokines TNF- α and IL-6 in serum from MI mice were detected by ELISA. As shown in Fig. 5D and E, both the levels of the two cytokines markedly increased in the MI group in comparison with the sham mice. The increases of IL-6 and TNF- α were remarkably suppressed with SOD-ZrMOF treatment.

The apoptosis ratio, determined by TUNEL staining, was significantly increased in all experimental groups 24 h after infarction, as shown in Fig. 5F and Figure S14. Similar to the results of *in vitro* experiments, SOD-ZrMOF treatments significantly mitigated the apoptosis ratio, suggesting that SOD-ZrMOF significantly increased the survival ratio of heart cells in the infarct area after MI.

3.8. Efficacy of SOD-ZrMOF in long-term cardiovascular disease model mice

In order to further investigate the long-term efficacy in MI mice, SOD-ZrMOF was intramyocardially injected into mice after permanent coronary artery occlusion, followed by normal housing and feeding for 4 weeks. To evaluate continuous changes in cardiac functions, echocardiography, a non-invasive method, was performed before MI and 7 days,

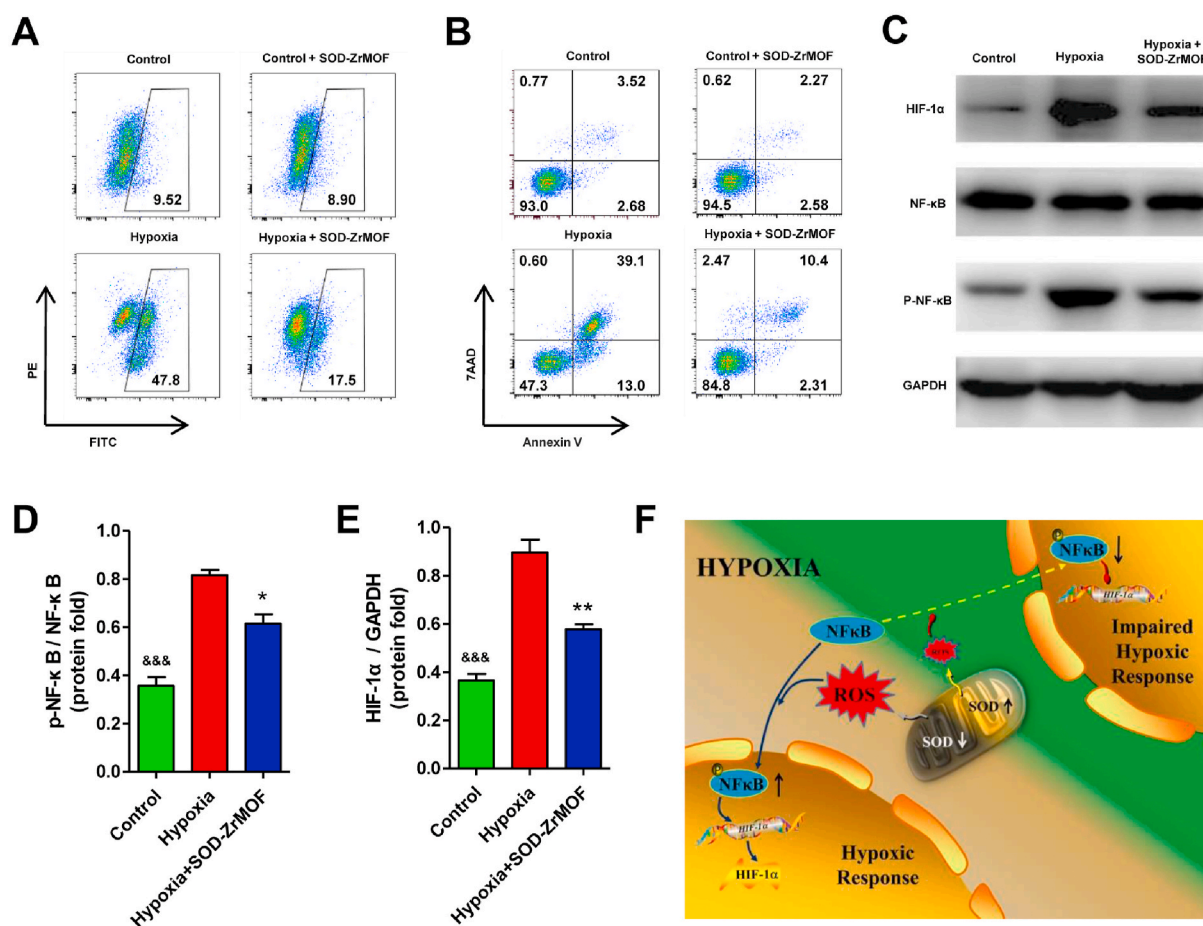


Fig. 4. Antioxidant activities of SOD-ZrMOF *in vitro*. (A) The MMP depolarization ratio was measured by JC-1 probe ($n = 3$). (B) The apoptosis and necrosis ratios of H9c2 cells after hypoxia were detected via Annexin V-FITC/PI double staining ($n = 3$). (C) NF- κ B and HIF-1 α expression before and after hypoxia with SOD-ZrMOF treatment was detected by Western blot. (D–E) Quantitative analysis of NF- κ B and HIF-1 α expression at the protein level. Mean \pm SD, $n = 3$. Compared to the hypoxia group, &&& indicates $P < 0.001$, * indicates $P < 0.05$, and ** indicates $P < 0.01$. (F) ROS regulates the expression of NF- κ B/HIF-1 α pathway in oxidative stress during hypoxia.

14 days, and 28 days after MI. Then, weight, heart weight, and tibia length were measured, and the hearts were collected to complete HE staining, Masson trichrome staining, sirius red staining, and immunohistochemical staining of α -SMA and CD31.

As shown in Fig. 6A–C, the EF% and FS% values in the MI group sharply decreased with time compared to the sham group. Strikingly, SOD-ZrMOF-treatment significantly suppressed the deterioration of these parameters after MI at all the different time points after MI. On the 28th day, to assess the ventricular remodeling of each group, the weight, heart weight and length of tibia were measured. No significant difference was found in body weight or tibia length among the three groups. However, in the MI group, the ratio of heart weight to body weight (HW/BW) (Figure S15a), as well as heart weight to tibia length (HW/TL) (Figure S15b), was notably raised in comparison with the sham group and MI group with SOD-ZrMOF treatment. The above two experiments prove that intramyocardial injection of SOD-ZrMOF improved the cardiac function both short-term and long-term after MI and effectively inhibited ventricular remodeling.

To probe the effects of SOD-ZrMOF on reducing infarct area and repressing fibrosis, HE staining, Masson trichrome staining and sirius red staining were used to measure the infarct area, left ventricle (LV) thickness, viable myocardium proportion, and fibrosis level 28 days after surgery (Fig. 6D). In comparison with the sham group, the proportions of the infarction area and collagen deposition in the MI group were increased to 30.3% and 11.4%, respectively. The type I collagen to type III ratio (I/III ratio) reached 2.06, and the LV thickness and viable

myocardium proportion were 0.16 mm and 20.3%, respectively. Consistently, SOD-ZrMOF treatment remarkably decreased the proportion of infarct area, collagen deposition, and I/III ratio to 12.4%, 5.7%, and 0.81, respectively, but the type III collagen proportion changed lightly. In addition, the LV thickness and viable myocardium proportion were increased to 0.47 mm and 41.4%, respectively (Figure S16–17).

Moreover, immunohistochemical staining of CD31 (red) and α -SMA (green) were measured to count density of vessel structures (Fig. 7A). As shown in Fig. 7B and C, both the expression of α -SMA and CD31 in the MI group changed slightly. However, there was a large increase of α -SMA and CD31 expression with SOD-ZrMOF treatment, suggesting that SOD-ZrMOF can promote angiogenesis in the heart after MI. In addition, the HE staining of the liver, spleen, lung, kidney, and non-MI area of the heart indicated that SOD-ZrMOF had no significantly toxicity in long term (Figure S18).

These long-term data demonstrated that, through promoting the survival of myocardial cells after MI, reducing the infarct area, promoting angiogenesis and inhibiting pathological myocardial remodeling, intramyocardial injection of SOD-ZrMOF may have excellent efficacy in reducing myocardial injury after MI.

4. Conclusion

An immobilized enzyme (SOD-ZrMOF) with the ability to efficiently scavenge ROS has been developed based on ZrMOF for the therapy of AMI. In short, SOD-ZrMOF shows excellent performance in eliminating

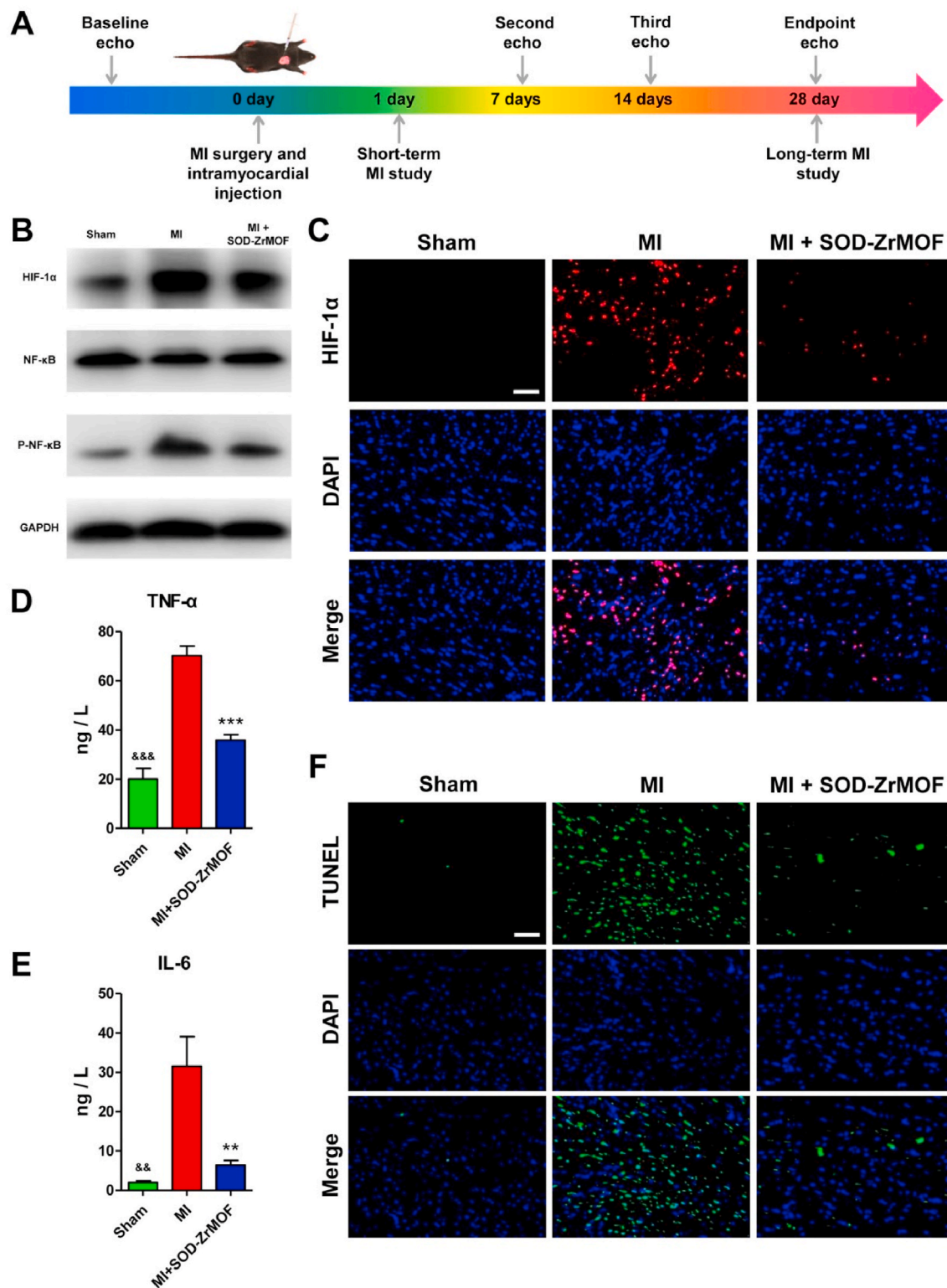


Fig. 5. Schematic of the entire design of animal study (A) and the efficacy of SOD-ZrMOF in mice 24 h after MI. (B) The NF-κB and HIF-1α expression was determined via western blotting (n = 3). (C) Immunohistochemistry staining of HIF-1α was used to assess myocardial hypoxia (scale bar: 50 μm, n = 5). Quantitative analysis of TNF-α (D) and IL-6 (E) in serum was detected using an ELISA kit. Mean ± SD, n = 5. &&& and ***P < 0.001, && and **P < 0.01, compared to the MI group. (F) 24 h after MI, cell apoptosis in the infarction area was detected using TUNEL staining (scale bar: 50 μm, n = 5).

ROS and protecting the function of mitochondria under hypoxia, and effectively inhibits the damage of cells induced by oxidative stress through repressing the NF-κB/HIF-1α pathway *in vitro*, and further reduced the death of CMs. *In vivo* results indicate that, by suppressing oxidative stress in the acute phase of MI, the injection of SOD-ZrMOF

into the affected cardiac tissue significantly reduces the death of CMs, further alleviating the amplifying effect of inflammation caused by CM death on myocardial damage. And in the chronic phase of ischemic remodeling after MI, SOD-ZrMOF still displayed strong cardioprotective effects, which effectively reduces infarct size, inhibits geometric changes

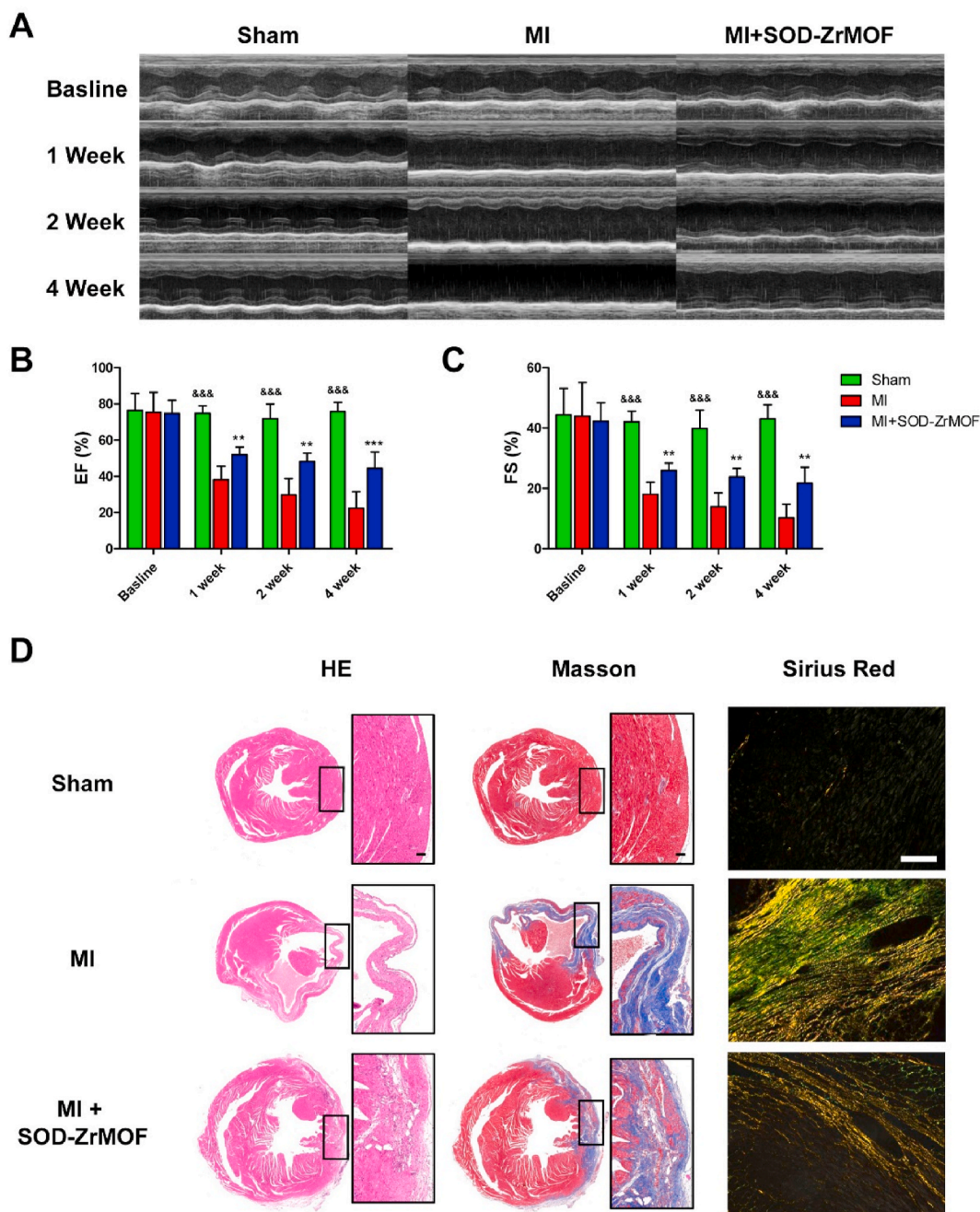


Fig. 6. The efficacy of SOD-ZrMOF in protecting cardiac function by decreasing infarct area and restraining pathological myocardial remodeling 28 days after MI. (A–C) Cardiac function indexes were determined by echocardiography. Mean \pm SD, $n = 6$. &&& and $***P < 0.001$, $**P < 0.01$, compared to the MI group. (D) HE, Masson trichrome staining (Scale bar: 200 μ m) and sirius red staining (Scale bar: 100 μ m) were used to observe the degree of MI and fibrosis ($n = 6$). (For interpretation of the references to color in this figure legend, the reader is referred to the Web version of this article.)

of the injured left ventricle, protects cardiac function, mitigates ventricular remodeling and promotes angiogenesis. In addition, preliminary *in vivo* studies show that SOD-ZrMOF is safe via intramyocardial injection.

Together, these characteristics prove the great potential of SOD-ZrMOF as an efficacious and safe nanomaterial option for the therapy of AMI, and SOD-ZrMOF deserves further development to treat numerous other ROS-related diseases.

Declaration of competing interest

The authors declare no conflict of interest.

CRediT authorship contribution statement

Jiacheng Guo: Methodology, Validation, Formal analysis, Roles, Writing – original draft. **Zhenzhen Yang:** Methodology, Validation, Formal analysis, Roles, Writing – original draft. **Yongzheng Lu:** Investigation, Writing – original draft. **Chunyan Du:** Investigation, Resources. **Chang Cao:** Formal analysis, Data curation. **Bo Wang:** Formal analysis, Data curation. **Xiaoting Yue:** Investigation. **Zenglei Zhang:** Investigation. **Yanyan Xu:** Investigation. **Zhen Qin:** Investigation. **Tingting Huang:** Conceptualization, Investigation, Formal analysis, Data curation. **Wei Wang:** Methodology, Validation, Formal analysis. **Wei Jiang:** Conceptualization, Investigation, Formal analysis, Data

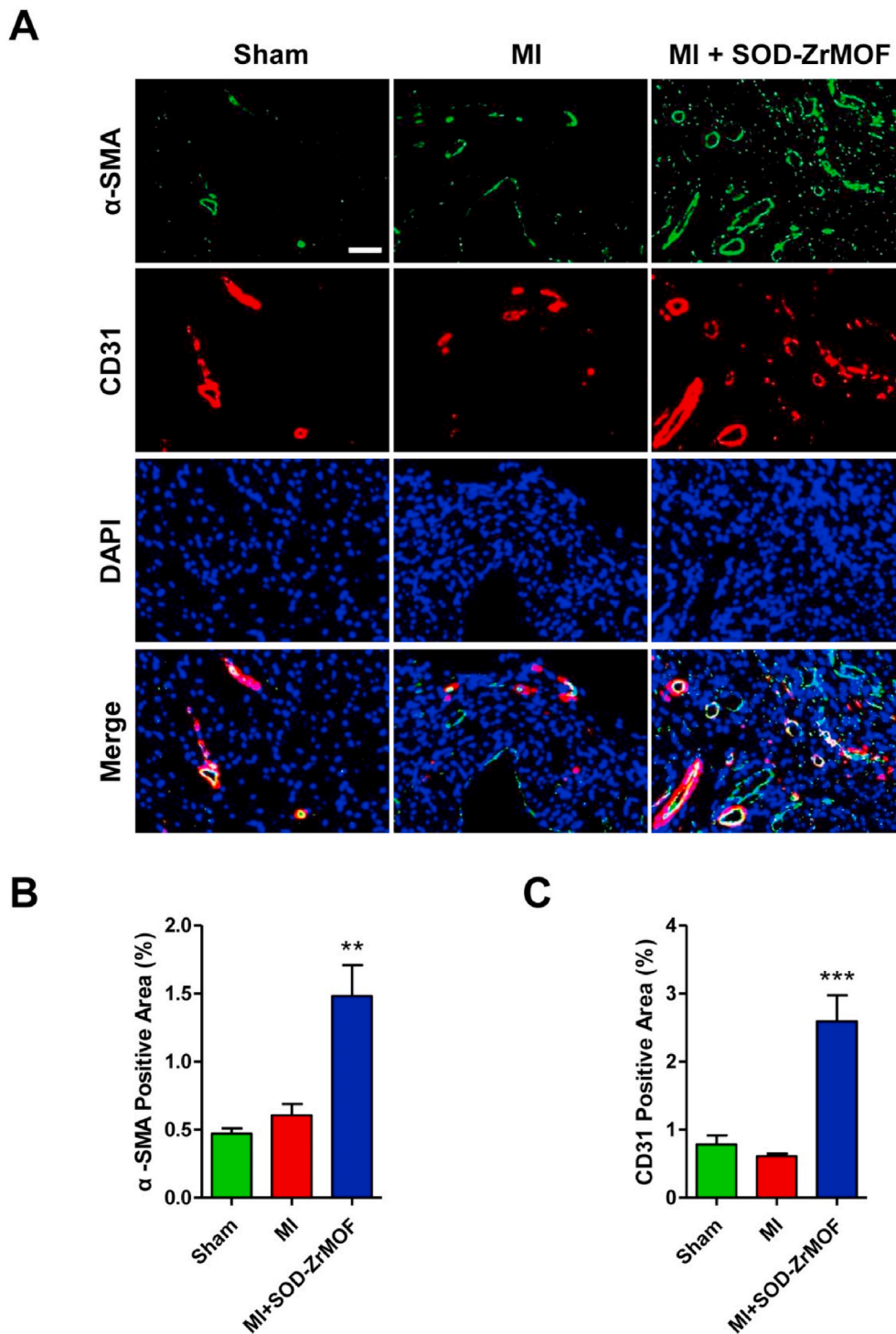


Fig. 7. The efficacy of SOD-ZrMOF in density of vessels was evaluated by α -SMA and CD31 staining. (A) Immunohistochemical staining of CD31 (red), α -SMA (green) and nuclei (blue) 28 days after MI. (B–C) Vessel structures density in tissues with PBS or SOD-ZrMOF treatment. Mean \pm SD. Scale bar: 50 μ m, n = 6. ** P < 0.01, *** P < 0.001. (For interpretation of the references to color in this figure legend, the reader is referred to the Web version of this article.)

curation, Writing – original draft, Writing – review & editing, Project administration. **Jinying Zhang:** Conceptualization, Writing – review & editing, Project administration, Funding acquisition. **Junnan Tang:** Conceptualization, Writing – original draft, Writing – review & editing, Project administration, Funding acquisition.

Acknowledgements

This work was supported by the National Natural Science Foundation of China (Grant Nos. 81870328, U2004203, 81800267, 82170281), Henan Thousand Talents Program (Grant No. ZYQR201912131), Henan Medical Science and Technology Joint Building Program (Grant No. 2018020002), Henan Province Youth Talent Promoting Project (Grant No. 2020HYTP051) and Excellent Youth Science Foundation of Henan

Province (Grant No. 202300410362). The authors also thank Miss Mengge Wu and Miss Shanshan Zhang for their assistance in the operation of animal experiments.

Appendix A. Supplementary data

Supplementary data to this article can be found online at <https://doi.org/10.1016/j.bioactmat.2021.08.019>.

References

- S.S. Virani, A. Alonso, E.J. Benjamin, M.S. Bittencourt, C.W. Callaway, A.P. Carson, et al., Heart disease and stroke statistics-2020 update: a report from the American heart association, *Circulation* 141 (2020) e139–e596, <https://doi.org/10.1161/CIR.0000000000000757>.
- Y. Nakada, D.C. Canseco, S. Thet, S. Abdisolaam, A. Asaithamby, C.X. Santos, et al., Hypoxia induces heart regeneration in adult mice, *Nature* 541 (2017) 222–227, <https://doi.org/10.1038/nature20173>.
- M. Bartekova, M. Barancik, K. Ferenczova, N.S. Dhalla, Beneficial effects of N-acetylcysteine and N-mercaptopyronylglycine on ischemia reperfusion injury in the heart, *Curr. Med. Chem.* 25 (2018) 355–366, <https://doi.org/10.2174/0929867324666170608111917>.
- M. Hori, K. Nishida, Oxidative stress and left ventricular remodeling after myocardial infarction, *Cardiovasc. Res.* 81 (2009) 457–464, <https://doi.org/10.1093/cvr/cvn335>.
- N.G. Frangogiannis, The inflammatory response in myocardial injury, repair, and remodeling, *Nat. Rev. Cardiol.* 11 (2014) 255–265, <https://doi.org/10.1038/nrcardio.2014.28>.
- T. Nishikido, J. Oyama, A. Shiraki, H. Komoda, K. Node, Deletion of apoptosis inhibitor of macrophage (AIM)/CD5L attenuates the inflammatory response and infarct size in acute myocardial infarction, *J. Am. Heart Assoc.* 5 (2016), e002863, <https://doi.org/10.1161/JAHA.115.002863>.
- I. Cabac-Pogorevici, B. Muk, Y. Rustamova, A. Kalogeropoulos, S. Tzeis, P. Vardas, Ischaemic cardiomyopathy. Pathophysiological insights, diagnostic management and the roles of revascularisation and device treatment. Gaps and dilemmas in the era of advanced technology, *Eur. J. Heart Fail.* 22 (2020) 789–799, <https://doi.org/10.1002/ejhf.1747>.
- J. Peng, D. Gurantz, V. Tran, R.T. Cowling, B.H. Greenberg, Tumor necrosis factor- α -induced AT1 receptor upregulation enhances angiotensin II-mediated cardiac fibroblast responses that favor fibrosis, *Circ. Res.* 91 (2002) 1119–1126, <https://doi.org/10.1161/01.res.0000047090.08299.d5>.
- L.H. Opie, P.J. Commerford, B.J. Gersh, M.A. Pfeffer, Controversies in ventricular remodeling, *Lancet* 367 (2006) 356–367, [https://doi.org/10.1016/S0140-6736\(06\)68074-4](https://doi.org/10.1016/S0140-6736(06)68074-4).
- T. Finkel, Signal transduction by reactive oxygen species, *J. Cell Biol.* 194 (2011) 7–15, <https://doi.org/10.1083/jcb.201102095>.
- B. D'Autreaux, M.B. Toledano, ROS as signalling molecules: mechanisms that generate specificity in ROS homeostasis, *Nat. Rev. Mol. Cell Biol.* 8 (2007) 813–824, <https://doi.org/10.1038/nrm2256>.
- T. Sciarbelli, A. Stephanou, N. Rayment, E. Pasini, L. Comini, S. Curello, et al., Apoptosis of endothelial cells precedes myocyte cell apoptosis in ischemia/reperfusion injury, *Circulation* 104 (2001) 253–256, <https://doi.org/10.1161/01.cir.104.3.253>.
- G.B. Waypa, J.D. Marks, M.M. Mack, C. Boriboun, P.T. Mungai, P.T. Schumacker, Mitochondrial reactive oxygen species trigger calcium increases during hypoxia in pulmonary arterial myocytes, *Circ. Res.* 91 (2002) 719–726, <https://doi.org/10.1161/01.res.0000036751.04896.f1>.
- G. Solaini, A. Baracca, G. Lenaz, G. Sgarbi, Hypoxia and mitochondrial oxidative metabolism, *Biochim. Biophys. Acta* 1797 (2010) 1171–1177, <https://doi.org/10.1016/j.bbabi.2010.02.011>.
- X.Q. Hu, L. Zhang, Hypoxia and mitochondrial dysfunction in pregnancy complications, *Antioxidants* 10 (2021), <https://doi.org/10.3390/antiox10030405>.
- Sousa Fialho, A.H. Abd Jamil, G.A. Stannard, L.C. Heather, Hypoxia-inducible factor 1 signalling, metabolism and its therapeutic potential in cardiovascular disease, *Biochim. Biophys. Acta (BBA) - Mol. Basis Dis.* 1865 (2019) 831–843, <https://doi.org/10.1016/j.bbadi.2018.09.024>.
- A. Chowdhury, A. Aich, G. Jain, K. Wozny, C. Luchtenborg, M. Hartmann, et al., Defective mitochondrial cardiolipin remodeling dampens HIF-1 α expression in hypoxia, *Cell Rep.* 25 (2018) 561–570 e6, <https://doi.org/10.1016/j.celrep.2018.09.057>.
- T. Hao, J. Li, F. Yao, D. Dong, Y. Wang, B. Yang, et al., Injectable fullerene/alginate hydrogel for suppression of oxidative stress damage in Brown adipose-derived stem cells and cardiac repair, *ACS Nano* 11 (2017) 5474–5488, <https://doi.org/10.1021/acsnano.7b00221>.
- Y. Yao, J. Ding, Z. Wang, H. Zhang, J. Xie, Y. Wang, et al., ROS-responsive polyurethane fibrous patches loaded with methylprednisolone (MP) for restoring structures and functions of infarcted myocardium in vivo, *Biomaterials* 232 (2020) 119726, <https://doi.org/10.1016/j.biomaterials.2019.119726>.
- L. Li, J. Guo, Y. Wang, X. Xiong, H. Tao, J. Li, et al., A broad-spectrum ROS-eliminating material for prevention of inflammation and drug-induced organ toxicity, *Adv. Sci.* 5 (2018) 1800781, <https://doi.org/10.1002/adv.201800781>.
- J.O. Defraigne, J. Pincemail, O. Detry, C. Franssen, M. Meurisse, R. Limet, Preservation of cortical microcirculation after kidney ischemia-reperfusion: value of an iron chelator, *Ann. Vasc. Surg.* 8 (1994) 457–467, <https://doi.org/10.1007/BF02133066>.
- R. Rodrigo, J.C. Prieto, R. Castillo, Cardioprotection against ischaemia/reperfusion by vitamins C and E plus n-3 fatty acids: molecular mechanisms and potential clinical applications, *Clin. Sci. (Lond.)* 124 (2013) 1–15, <https://doi.org/10.1042/CS20110663>.
- L. Lin, H. Gong, R. Li, J. Huang, M. Cai, T. Lan, et al., Nanodrug with ROS and pH dual-sensitivity ameliorates liver fibrosis via multicellular regulation, *Adv. Sci.* 7 (2020) 1903138, <https://doi.org/10.1002/adv.201903138>.
- D.P. Riley, Functional mimics of superoxide dismutase enzymes as therapeutic agents, *Chem. Rev.* 99 (1999) 2573–2588, <https://doi.org/10.1021/cr980432g>.
- D. Salvemini, D.P. Riley, S. Cuzzocrea, SOD mimetics are coming of age, *Nat. Rev. Drug Discov.* 1 (2002) 367–374, <https://doi.org/10.1038/nrd796>.
- W. Liang, P. Wied, F. Carraro, C.J. Sumbly, B. Nidetzky, C.K. Tsung, et al., Metal-organic framework-based enzyme biocomposites, *Chem. Rev.* 121 (2021) 1077–1129, <https://doi.org/10.1021/acs.chemrev.0c01029>.
- J.M. Guisan, J.M. Bolivar, F. Lopez-Gallego, J. Rocha-Martin, Correction to: immobilization of enzymes and cells, *Methods Mol. Biol.* 2100 (2020) C1, https://doi.org/10.1007/978-1-0716-0215-7_33.
- A. Kuchler, M. Yoshimoto, S. Luginbuhl, F. Mavelli, P. Walde, Enzymatic reactions in confined environments, *Nat. Nanotechnol.* 11 (2016) 409–420, <https://doi.org/10.1038/nnano.2016.54>.
- A. Schaate, P. Roy, A. Godt, J. Lippke, F. Waltz, M. Wiebcke, et al., Modulated synthesis of Zr-based metal-organic frameworks: from nano to single crystals, *Chemistry* 17 (2011) 6643–6651, <https://doi.org/10.1002/chem.201003211>.
- W. Jiang, X. Wang, J. Chen, Y. Liu, H. Han, Y. Ding, et al., Deuterohemin-peptide enzyme mimic-embedded metal-organic frameworks through biomimetic mineralization with efficient ATRP catalytic activity, *ACS Appl. Mater. Interfaces* 9 (2017) 26948–26957, <https://doi.org/10.1021/acsami.7b09218>.
- R. Ventura-Clapier, A. Garnier, V. Veksler, Energy metabolism in heart failure, *J. Physiol.* 555 (2004) 1–13, <https://doi.org/10.1113/jphysiol.2003.055095>.
- J.M. Suski, M. Lebedzinska, M. Bonora, P. Pinton, J. Duszynski, M.R. Wieckowski, Relation between mitochondrial membrane potential and ROS formation, *Methods Mol. Biol.* 810 (2012) 183–205, https://doi.org/10.1007/978-1-61779-382-0_12.
- J. Zou, Y. Zhang, J. Sun, X. Wang, H. Tu, S. Geng, et al., Deoxyephantopin induces reactive oxygen species-mediated apoptosis and autophagy in human osteosarcoma cells, *Cell. Physiol. Biochem.* 42 (2017) 1812–1821, <https://doi.org/10.1159/000479537>.
- J.W. Gordon, J.A. Shaw, L.A. Kirshenbaum, Multiple facets of NF- κ B in the heart: to be or not to NF- κ B, *Circ. Res.* 108 (2011) 1122–1132, <https://doi.org/10.1161/CIRCRESAHA.110.226928>.
- T. Bishop, P.J. Ratcliffe, HIF hydroxylase pathways in cardiovascular physiology and medicine, *Circ. Res.* 117 (2015) 65–79, <https://doi.org/10.1161/CIRCRESAHA.117.305109>.
- G.L. Semenza, Oxygen sensing, hypoxia-inducible factors, and disease pathophysiology, *Annu. Rev. Pathol.* 9 (2014) 47–71, <https://doi.org/10.1146/annurev-pathol-012513-104720>.
- Z. Liu, Y. Huang, Y. Jiao, Q. Chen, D. Wu, P. Yu, et al., Polystyrene nanoplastic induces ROS production and affects the MAPK-HIF-1/NF κ B-mediated antioxidant system in *Daphnia pulex*, *Aquat. Toxicol.* 220 (2020) 105420, <https://doi.org/10.1016/j.aquatox.2020.105420>.
- S.E. Corcoran, L.A. O'Neill, HIF1 α and metabolic reprogramming in inflammation, *J. Clin. Invest.* 126 (2016) 3699–3707, <https://doi.org/10.1172/JCI84431>.
- M. Wartenberg, S. Gronczynska, M.M. Bekhite, T. Saric, W. Niedermeier, J. Hescheler, et al., Regulation of the multidrug resistance transporter P-glycoprotein in multicellular prostate tumor spheroids by hyperthermia and reactive oxygen species, *Int. J. Canc.* 113 (2005) 229–240, <https://doi.org/10.1002/ijc.20596>.
- S. Bonello, C. Zahringer, R.S. BelAiba, T. Djordjevic, J. Hess, C. Michiels, et al., Reactive oxygen species activate the HIF-1 α promoter via a functional NF κ B site, *Arterioscler. Thromb. Vasc. Biol.* 27 (2007) 755–761, <https://doi.org/10.1161/01.ATV.0000258979.92828.bc>.
- S.W. Leuthauser, L.W. Oberley, T.D. Oberley, J.R. Sorenson, K. Ramakrishna, Antitumor effect of a copper coordination compound with superoxide dismutase-like activity, *J. Natl. Cancer Inst.* 66 (1981) 1077–1081, <https://doi.org/10.1093/jnci/66.6.1077>.
- R. Esco, J. Valencia, P. Coronel, J.A. Carceller, M. Gimeno, N. Bascon, Efficacy of orgetein in prevention of late side effects of pelvic irradiation: a randomized study, *Int. J. Radiat. Oncol. Biol. Phys.* 60 (2004) 1211–1219, <https://doi.org/10.1016/j.ijrobp.2004.04.038>.
- J. Noda, M. Otogiri, T. Akaike, H. Maeda, Pharmacological advantages of conjugation of Cu, Zn-superoxide dismutase with succinylated keratin fragment: improvement of biological properties and resistance to oxidative damage, *J. Pharmacol. Exp. Therapeut.* 279 (1996) 162–171.